Journal of Cleaner Production 265 (2020) 121502

Contents lists available at ScienceDirect

Journal of Cleaner Production

journal homepage: www.elsevier.com/locate/jclepro

A novel waste heat recovery system combing steam Rankine cycle and organic Rankine cycle for marine engine

Xiangyang Liu [a], Manh Quang Nguyen [a, b], Jianchu Chu [a], Tian Lan [a], Maogang He [a, *]

[a] MOE Key Laboratory of Thermal-Fluid Science and Engineering, School of Energy and Power Engineering, Xi'an Jiaotong University, Xi'an, 710049, China
[b] Le Quy Don Technical University, Hanoi, 122314, Viet Nam

ARTICLE INFO

Article history:
Received 13 July 2019
Received in revised form
26 March 2020
Accepted 1 April 2020
Available online 14 April 2020

Handling editor. Prof. Jiri Jaromir Klemeš

Keywords:
Steam Rankine cycle
Organic Rankine cycle
Marine engine
Waste heat utilization

ABSTRACT

Aiming to reduce fuel consumption and pollutant emission, a new kind of waste heat recovery system (WHRS) is proposed to recycle the waste heat of marine engine. In the proposed system, steam and organic Rankine cycles are combined to convert the waste heat of the exhaust gas and jacket cooling water of marine engine into mechanical energy. A portion of the jacket cooling water is used as the working fluid for the steam Rankine cycle subsystem to efficiently utilize the heat of jacket cooling water and avoid increased ship weight caused by the extra water. The performance of the proposed system for recovering the waste heat of a 14-cylinder two-stroke marine engine was simulated and compared to performance of the WHRSs based on a single steam Rankine cycle (SSRC) and a dual pressure organic Rankine cycle (DPORC). The results show that the proposed system could improve the thermal efficiency of engine by 4.42% and reduce the fuel consumption by 9322 tons per year at an engine load of 100%, while a WHRS based on a SSRC and a DPORC can only increase the thermal efficiency by 2.68% and 3.42%, respectively. In addition, effects of evaporation pressure, the degree of superheat and engine load on the output work, the exergy destruction rate, and the thermal and exergy efficiency of the proposed system were analyzed to provide information for system optimization.

1. Introduction

The volume of world trade is rapidly increasing, and most of volume is transported through ship (Mondejar et al., 2018). Heavy fuel consumption is required to provide power for the ships, which greatly contributes to the oil crisis (Shu et al., 2013) and environmental pollution (Corbett et al., 2007). Currently, approximately half of the heat from fuel combustion in a marine engine is discharged into the environment along with exhaust gas (EG) and jacket cooling water (JCW), *etc.* (Shu et al., 2013). If this portion of the heat can be recovered, the thermal efficiency of marine engine can be increased and fuel consumption and pollution emission can be reduced.

There are two ways to reduce the fossil fuel consumption and environmental pollution. One way is to develop renewable energy sources like biofuel (Liu et al., 2019a), geothermal energy (Parikhani et al., 2019), solar energy (Liu et al., 2019b), and clean working fluid (Liu et al., 2019c). Another is to recover the waste heat during the energy conversion process utilizing technology such as organic Rankine cycle (ORC) (Zhang et al., 2018), absorption refrigeration (Liu et al., 2019d), and Kalina cycle (Ghaebi et al., 2018). An earlier publication (Singh and Pedersen, 2016) reviewed different types of technologies for marine engines. These technologies including steam Rankine cycle (SRC) (Theotokatos and George, 2013), ORC (Ng et al., 2019), Kalina cycle (Larsen et al., 2014), absorption refrigeration (Salmi et al., 2017), and their combinations (Patel et al., 2017). They have been utilized to convert the waste heat of marine engines to electrical energy, heat energy or mechanical energy. SRC is a well-established technology (Mondejar et al., 2018), but its thermal efficiency is very low when it is driven by heat lower than 200 °C. Compared to SRC, ORC better utilizes waste heat at lower temperatures (Jankowski et al., 2019). Therefore, considerable effort has been put into developing WHRS based on ORC to recover the waste heat of EG, scavenge air, JCW, and lubricating oil of marine engines. Baldasso et al. (2019) studied the effect of the equipment for nitrogen oxide emission reduction with respect to power generation, heat exchanger volume, and cost of a WHRS based on ORC for a feeder ship. Zhu et al. (2018) optimized the parameters of a WHRS based on the ORC for EG of marine engine

* Corresponding author.
E-mail address: mghe@mail.xjtu.edu.cn (M. He).

https://doi.org/10.1016/j.jclepro.2020.121502
0959-6526/

Nomenclature

h	Enthalpy ($kJ \cdot kg^{-1}$)
t	Temperature (°C)
T	Temperature (K)
W	Work (kw)
Q	Heat load (kw)
I	Exergy destruction rate (kw)
m	Mass flow rate ($kg \cdot s^{-1}$)
c_p	Isobaric specific heat capacity ($kJ \cdot kg^{-1} \cdot K^{-1}$)
s	Entropy ($kJ \cdot kg^{-1} \cdot K^{-1}$)

Abbreviations

SRC	Steam Rankine cycle
ORC	Organic Rankine cycle
WHRS	Waste heat recovery system
SSRC	WHRS based on single SRC
DPORC	WHRS based on dual pressure ORC
SORC	WHRS designed in this work
JCW	Jacket cooling water
EG	Exhaust gas

Greak symbols

η	Efficiency
ε	Isentropic efficiency

Subscripts

eg	Exhaust gas
w1	JCW for SRC
w2	JCW for preheater
he1	Heat exchanger 1
he2	Heat exchanger 2
ave1	Average temperature of EG in Heat exchanger 1
ave2	Average temperature of EG in Heat exchanger 2
tu	Turbine
cn	Condenser n
pn	Pump n
ex	Expander
E	Exergy
OF	Working fluid for ORC
0	Ambient condition
SRC	Steam Rankine cycle
ORC	Organic Rankine cycle
cw	Cooling water
in	Input
out	Output
pre	Preheater
ds	Degree of superheat

considering the thermodynamic and economic performance. Yang and Yeh (2015) investigated the thermodynamic and economic performance of a WHRS based on the ORC for marine engine, and R1234yf showed the best performance among the six working fluids. Shu et al. (2017) presented an operational profile for evaluating the thermodynamic and economic performance of a WHRS based on the ORC for marine engine to utilize the heat of EG. Girgin and Ezgi (2017) used a WHRS based on the ORC with a generator to utilize the heat of EG of a naval ship, and seven working fluids containing R123, R141b, isopentane, n-pentane, n-hexane, benzene, and toluene were tested. Soffiato et al. (2015) compared the thermodynamic performance of WHRS based on the ORC, the regenerated ORC, and a dual pressure ORC for recycling the waste heat of the engine of liquefied natural gas carrier. Yang (2016) used a WHRS based on a transcritical ORC to utilize the waste heat of a marine engine. Six working fluids containing two HFOs, three HFCs and R290 were tested. Andreasen et al. (2017) compared the performance of a dual pressure SRC and an ORC for recovery of waste heat of EG, scavenge air and JCW of marine engine. Uusitalo et al. (2019) used the heat of EG of a cruise ship to provide steam, which was utilized to heat consumers and generate electrical energy by the SRC and the ORC.

For some ships, the temperature of EG from their engine is above 250 °C where SRC has better performance than ORC. In this case, ORC can be combined with SRC to achieve greater efficiency of EG heat usage. Nielsen et al. (2014) developed a WHRS containing SRC and ORC to recover the heat of EG from a two-stroke diesel engine. Choi and Young (2013) proposed a dual loop WHRS integrating SRC with ORC to utilize the heat of EG of 6800 TEU (Twenty-foot Equivalent Unit) container ship.

JCW from a marine engine has a large amount of low temperature waste heat, which is not easily recovered. As reviewed by Mondejar et al. (2018), previous publications only used a single ORC or SRC to recover the waste heat of JCW, or together with that of EG. The results show that the recovery efficiency of high- or low-temperature waste heat is relatively low. Combining the ORC with the SRC to gradually recover the waste heat of JCW and EG can overcome this problem, however, no studies on this method have been discovered. The EG first provides heat to the evaporator of the SRC and then continues to provide heat to the evaporator of the ORC, indicating that the heat distribution between the two cycles has an important effect on the cycle performance, however, no optimization work has been performed.

In order to improve the degree of utilization of the waste heat of marine engines, a new WHRS is proposed in this paper, which combines the SRC and the ORC to gradiently utilizes the heat of the EG and JCW. In the proposed system, a portion of the JCW is used as the working fluid of the SRC subsystem to efficiently utilize the JCW heat and avoid increased ship weight caused by the extra water. The thermodynamic performance of the proposed WHRS for recovering the waste heat of a two-stroke marine engine is analyzed.

2. The new waste heat recovery system

Fig. 1 is a schematic diagram of the new WHRS (SORC) proposed herein. It contains an SRC subsystem and an ORC subsystem. The SRC and ORC subsystems are used to recover the high and low temperature heat of the EG, respectively, while they recover the heat of the JCW by using it as working and preheating fluid, respectively. In the SRC subsystem, a portion of the JCW from the marine engine is heated to become superheated steam by the high-temperature EG discharged from the engine. The superheated steam enters the turbine to output work, which drives the generator to generate electrical energy. It then enters Condenser 1 to be condensed into liquid water. Because the amount of JCW is very large, the SRC subsystem cannot fully utilize all of it. Thus, the working fluid for the ORC is preheated by a portion of the JCW from the engine, with the intent to utilize the waste heat of the JCW to improve the ORC output work efficiency. The working fluid is then heated further by the EG in Heat Exchanger 2. JCW from the preheater and Condenser 1 are blended and cooled in Condenser 3. Then the JCW enters the engine to absorb heat. The temperature of the JCW must be higher than 60 °C before entering the marine engine. If the temperature of the JCW is too low, the cylinder and

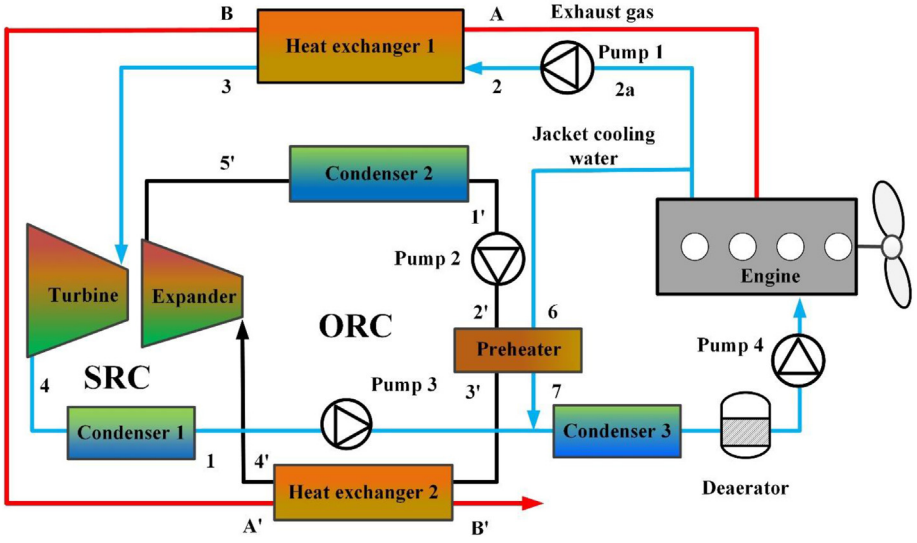

Fig. 1. Schematic diagram of the proposed WHRS.

combustion temperature will be low and the output work of the engine will be reduced. A deaerator is used to remove the non-condensable gases from the JCW before entering the engine.

Thermodynamic properties of working fluid have an important influence on the performance of the ORC (Uusitalo et al., 2018). Based on the previous results (He et al., 2011), cyclopentane is chosen as the working fluid for the ORC subsystem. The discharge temperature of EG at the outlet of Heat Exchanger 2 was set to a minimum of 140 °C, because the acid dew point temperature of approximately 130 °C can have a negative impact on the equipment and needs to be taken into consideration.

3. Thermodynamic model of the new waste heat recovery system

In order to clearly describe the thermodynamic process of the working fluids in the new WHRS, the temperature-entropy diagram is shown in Fig. 2. To simplify the simulation, the following assumptions were made: (1) the system was in a steady state and (2) the pressure drop and heat loss in heat exchangers and pipes was negligible.

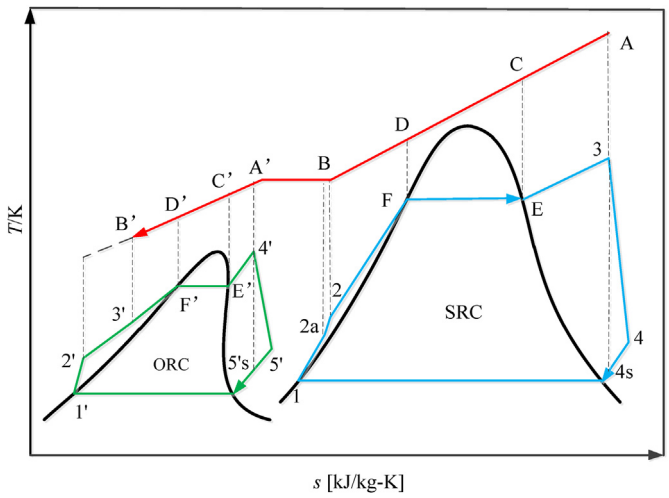

Fig. 2. *T-s* diagram of the proposed WHRS.

3.1. Thermodynamic model of steam Rankine cycle subsystem

After the JCW comes out from engine, it is pressurized by pump. The electrical power consumed by the Pump 1 (W_{p1}) and exergy destruction rate (I_{p1}) caused by the Pump 1 are calculated by

$$W_{p1} = \frac{m_{w1}(h_2 - h_{2a})}{\varepsilon_{p1}} \tag{1}$$

$$I_{p1} = m_{w1} T_0 (s_2 - s_{2a}) \tag{2}$$

where ε_{p1} is the isentropic efficiency of Pump 1; m_{w1} is mass flow rate of the JCW in the SRC; h_2 and h_{2a} are the enthalpies of the JCW at Point 2 and Point 2a, respectively; s_2 and s_{2a} are the entropies of the JCW at Point 2 and Point 2a, respectively; T_0 is environment temperature. m_{w1} can be obtained by

$$m_{eg} c_{p,eg} (T_A - T_D) = m_{w1} (h_3 - h_F) \tag{3}$$

where m_{eg} is mass flow rate of EG; $c_{p,eg}$ is the isobaric specific heat capacity of EG, T_A and T_D are temperatures of EG at Point A and Point D, respectively; h_3 and h_F are the enthalpies of the JCW at Point 3 and Point F, respectively. T_D can be obtained by pinch point temperature and T_F.

In Heat Exchanger 1, the JCW absorbs heat from EG and evaporates into steam, which is an isobaric process. The temperature of the JCW at the inlet of Heat Exchanger 1 is equal to the temperature of the JCW at the outlet of the engine. The JCW at the outlet of Heat Exchanger 1 is in a superheated state. The heat absorbed by the JCW (Q_{he1}) and the exergy destruction rate (I_{eg1}) of EG during the heat exchange process are calculated by

$$Q_{he1} = m_{w1} (h_3 - h_2) \tag{4}$$

$$I_{eg1} = Q_{he1} \left(1 - \frac{T_0}{T_{ave1}}\right) \tag{5}$$

where h_2 is the enthalpy of the JCW at Point 2. T_{ave1} is the average temperature of EG in Heat Exchanger 1, which is calculated by

$$T_{ave1} = \frac{T_A - T_B}{\ln \frac{T_A}{T_B}} \tag{6}$$

The exergy destruction rate of the JCW in Heat Exchanger 1 (I_{w1}) is

$$I_{w1} = m_{w1}(h_2 - h_3 - T_0(s_2 - s_3)) \tag{7}$$

where s_2 and s_3 are the entropies of the JCW at Point 2 and Point 3, respectively.

The exergy destruction rate of Heat Exchanger 1 (I_{he1}) is

$$I_{he1} = I_{eg1} + I_{w1} \tag{8}$$

At the outlet of Heat Exchanger 1, the water becomes high-temperature and high-pressure steam and goes into the turbine to output work (W_{tu}), which is calculated by

$$W_{tu} = m_{w1}(h_3 - h_{4s})\varepsilon_{tu} = m_{w1}(h_3 - h_4) \tag{9}$$

where ε_{tu} is the isentropic expansion efficiency of the turbine; and h_{4s} is the enthalpy of the JCW at the turbine outlet when an isentropic expansion process is proceeding.

The output work of the SRC subsystem (W_{SRC}) is calculated by

$$W_{SRC} = W_{tu} - W_{p1} \tag{10}$$

The exergy destruction rate of turbine (I_{tu}) is calculated by

$$I_{tu} = m_{w1}T_0(s_4 - s_3) \tag{11}$$

where s_4 is the entropy of the JCW at Point 4.

The steam from the turbine outlet enters Condenser 1 and is condensed into a liquid state. The heat released from the steam during the condensation process (Q_{c1}) is calculated by

$$Q_{c1} = m_{w1}(h_4 - h_1) \tag{12}$$

The exergy destruction rate in Condenser 1 (I_{c1}) is

$$I_{c1} = m_{cw1}\left(h_{cw1,in} - h_{cw1,out} - T_0\left(s_{cw1,in} - s_{cw1,out}\right) + m_{w1}(h_4 - h_1 - T_0(s_4 - s_1)\right) \tag{13}$$

where $h_{cw1,\,out}$ and $h_{cw1,\,in}$ are the enthalpies of cooling water at the outlet and inlet of Condenser 1, respectively; $s_{cw1,\,out}$ and $s_{cw1,\,in}$ are the entropies of cooling water at the outlet and inlet of Condenser 1, respectively; and m_{cw1} is the mass flow rate of cooling water. The thermal efficiency (η_{SRC}), the exergy destruction rate (I_{SRC}), and the exergy efficiency ($\eta_{E,SRC}$) of the SRC subsystem are calculated by

$$\eta_{SRC} = \frac{W_{SRC}}{Q_{he1}} \tag{14}$$

$$I_{SRC} = I_{p1} + I_{he1} + I_{tu} + I_{c1} \tag{15}$$

$$\eta_{E,1} = \frac{W_{SRC}}{W_{SRC} + I_{SRC}} \tag{16}$$

3.2. Thermodynamic model of organic Rankine cycle subsystem

In the preheater, the heat exchange amount (Q_{pre}) and exergy destruction rate (I_{pre}) are calculated by

$$Q_{pre} = m_{w2}(h_6 - h_7) = m_{OF}(h_{3'} - h_{2'}) \tag{17}$$

$$I_{pre} = m_{w2}(h_6 - h_7 - T_0(s_6 - s_7)) + m_{OF}(h_{2'} - h_{3'} - T_0(s_{2'} - s_{3'}) \times) \tag{18}$$

where m_{OF} and m_{w2} are the mass flow rate of cyclopentane and the JCW through the preheater, respectively; h_6 and $h_{7,}$ are the enthalpies of the JCW at points 6 and 7, respectively; $h_{2'}$ and $h_{3'}$ are the enthalpies of cyclopentane at points 2′ and 3′, respectively; s_6 and s_7 are the entropies of the JCW at points 6 and 7, respectively; and $s_{2'}$ and $s_{3'}$ are the entropies of cyclopentane at points 2′ and 3′, respectively.

The amount of heat exchange in Heat Exchanger 2 (Q_{he2}) is

$$Q_{he2} = m_{OF}(h_{4'} - h_{3'}) \tag{19}$$

where $h_{4'}$ is the enthalpy of cyclopentane at point 4'. The heat exchange process in Heat Exchanger 2 meets eq. (20), therefore m_{OF} can be calculated by eq (21).

$$m_{eg}c_{p,eg}(T_{A'} - T_{D'}) = m_{OF}(h_{4'} - h_{F'}) \tag{20}$$

$$m_{OF} = \frac{m_{eg}c_{p,eg}(T_{A'} - T_{D'})}{h_{4'} - h_{F'}} \tag{21}$$

where $T_{A'}$ and $T_{D'}$ are temperatures of the EG at points A′ and D'; $h_{F'}$ is the enthalpy of cyclopentane at point F'. $T_{A'}$ equals the temperature of the EG at the outlet of Heat Exchanger 1. The exergy destruction rate in Heat Exchanger 2 (I_{he2}) is calculated by

$$I_{he2} = Q_{he2}\left(1 - \frac{T_0}{T_{ave2}}\right) + m_{OF}(h_{3'} - h_{4'} - T_0(s_{3'} - s_{4'})) \tag{22}$$

where $s_{4'}$ is the entropy of cyclopentane at point 4'. T_{ave2} is the average temperature of the EG in Heat Exchanger 2.

The output work (W_{ex}) and the exergy destruction rate (I_{ex}) of the expander are calculated by eq (23) and eq (24).

$$W_{ex} = m_{OF}(h_{4'} - h_{5'}) = m_{OF}\varepsilon_{ex}(h_{4'} - h_{5's}) \tag{23}$$

$$I_{ex} = m_{OF}T_0(s_{5'} - s_{4'}) \tag{24}$$

where $h_{5'}$ and $s_{5'}$ are the enthalpy and entropy of cyclopentane at point 5′, respectively; $h_{5's}$ is the enthalpy of cyclopentane at the outlet of the expander when an isentropic expansion process is proceeding; ε_{ex} is the isentropic expansion efficiency of the expander.

The heat exchange amount of Condenser 2 (Q_{c2}) is calculated by

$$Q_{c2} = m_{OF}(h_{5'} - h_{1'}) \tag{25}$$

where $h_{1'}$ is the enthalpy of cyclopentane at point 1'.

The exergy destruction rate of Condenser 2 (I_{c2}) is calculated by

$$I_{c2} = m_{cw2}\left(h_{cw2,in} - h_{cw2,out} - T_0\left(s_{cw2,in} - s_{cw2,out}\right) + m_{OF}(h_{5'} - h_{1'} - T_0(s_{5'} - s_{1'})\right) \tag{26}$$

where m_{cw2} is the as the cooling water enters into Condenser 2; $h_{cw2,\,out}$ and $h_{cw2,\,in}$ are the enthalpies of the cooling water at the outlet and inlet of Condenser 2, respectively; $s_{cw2,\,out}$ and $s_{cw2,\,in}$ are the entropies of the cooling water at the outlet and inlet of

Table 1
The mass flow rate and temperature of EG from engine under different loads.

Engine load/%	Engine power/kW	Mass Flow rate of EG/(kg·s^{-1})	Temperature of EG/°C
110	92,708	223.4	287.4
100	84,280	202.0	284.0
95	80,066	191.3	282.5
90	75,852	180.6	281.0
85	71,638	170.1	279.2
80	67,424	159.5	277.3
75	63,210	148.9	275.1
70	58,996	138.4	273.2
65	54,782	127.9	271.0
60	50,568	117.5	268.6
55	46,354	107.1	266.3
50	42,140	96.9	263.2
45	37,926	86.6	259.6
40	33,712	76.4	256.8
35	29,498	66.2	253.2
30	25,284	56.1	248.1

Table 2
Parameters of SORC.

Parameter	Value
Condensation temperature of SRC	46 °C
Condensation temperature of ORC	38 °C
Ambient temperature	25 °C
Pinch point temperature in heat exchanger 1	25 °C
Pinch point temperature in preheater	6 °C
Isentropic efficiency of pump	0.8
Isentropic efficiency of expander and turbine	0.8
Temperature of cooling water	25 °C
Pinch point temperature in condenser 1 and condenser 2	6 °C

Condenser 2, respectively; $s_{1'}$ is the entropy of cyclopentane at point 1'.

The power consumed by Pump 2 (W_{p2}) is calculated by

$$W_{p2} = \frac{m_{OF}(h_{2'} - h_{1'})}{\varepsilon_{p2}} \tag{27}$$

where ε_{p2} is the isentropic efficiency of Pump 2. The exergy destruction rate caused by Pump 2 (I_{p2}) is calculated by

$$I_{p2} = m_{OF}T_0(s_{2'} - s_{1'}) \tag{28}$$

The output work of the ORC subsystem (W_{ORC}) is calculated by

$$W_{ORC} = W_{ex} - W_{p2} \tag{29}$$

The exergy destruction rate of ORC subsystem is calculated by

$$I_{ORC} = I_{pre} + I_{he2} + I_{ex} + I_{c2} + I_{p2} \tag{30}$$

The thermal efficiency (η_{ORC}) and exergy efficiency ($\eta_{E,ORC}$) of the ORC subsystem is calculated by

$$\eta_{ORC} = \frac{W_{ORC}}{Q_{he2} + Q_{pre}} \tag{31}$$

$$\eta_{E,ORC} = \frac{W_{ORC}}{W_{ORC} + I_{ORC}} \tag{32}$$

The total output work of the SORC (W_{SORC}) is calculated by

$$W_{SORC} = W_{SRC} + W_{ORC} \tag{33}$$

The thermal efficiency of the SORC (η) is calculated by

$$\eta = \frac{W_{SORC}}{Q_{he1} + Q_{he2} + Q_{pre}} \tag{34}$$

The exergy efficiency of the SORC (η_E) is calculated by

$$\eta_E = \frac{W_{SORC}}{W_{SORC} + I_{SRC} + I_{ORC}} \tag{35}$$

4. Analysis of thermodynamic performance of waste heat utilization system

In this paper, a two-stroke marine engine MAN B&W−14K98ME-C7.1-TII was selected as the research object to evaluate the thermodynamic performance of the SORC. The temperature of the JCW at the engine outlet is 85 °C, which does not change under different loads. However, the temperature of the EG from the engine changes significantly under different engine loads. Table 1 gives the temperature and mass flow rate of the EG from the engine under different engine loads, which is calculated by the method provided in the MAN B&W K98ME-C7.1-TII manual (2014).

Using the thermodynamic model established above, the thermodynamic performance of the SORC under different working conditions was calculated and analyzed. The calculation is carried out using the program written in MATLAB. Table 2 shows some recommended system parameters used during the calculation process (Andreasen et al., 2015; Song et al., 2015).

The evaporation pressure of the SRC subsystem has an important influence on the thermodynamic performance of the SORC. The output work, thermal and exergy efficiencies of the SRC subsystem, and the ORC subsystem under different evaporation pressures of the SRC subsystem at the engine load of 100% were calculated and are shown in Fig. 3. Pinch point temperature in heat exchanger 2, EG discharge temperature, and the degree of superheat are set to 10 °C, 140 °C, and 25 °C, respectively. Fig. 3(a) illustrates that as the evaporation pressure of the SRC subsystem increases, the output work of the SRC subsystem first rises and then falls; it reaches a maximum value when the evaporation pressure is around 0.55 MPa. This is because when the evaporation pressure of the SRC subsystem increases, the water at the outlet of heat exchanger 1 is at a higher temperature. Therefore, the thermal efficiency of the SRC subsystem increases, but the heat of the EG input into the SRC subsystem decreases. Meanwhile, additional heat of the EG is input into the ORC subsystem as the evaporation pressure of the SRC subsystem increases, which results in increased output

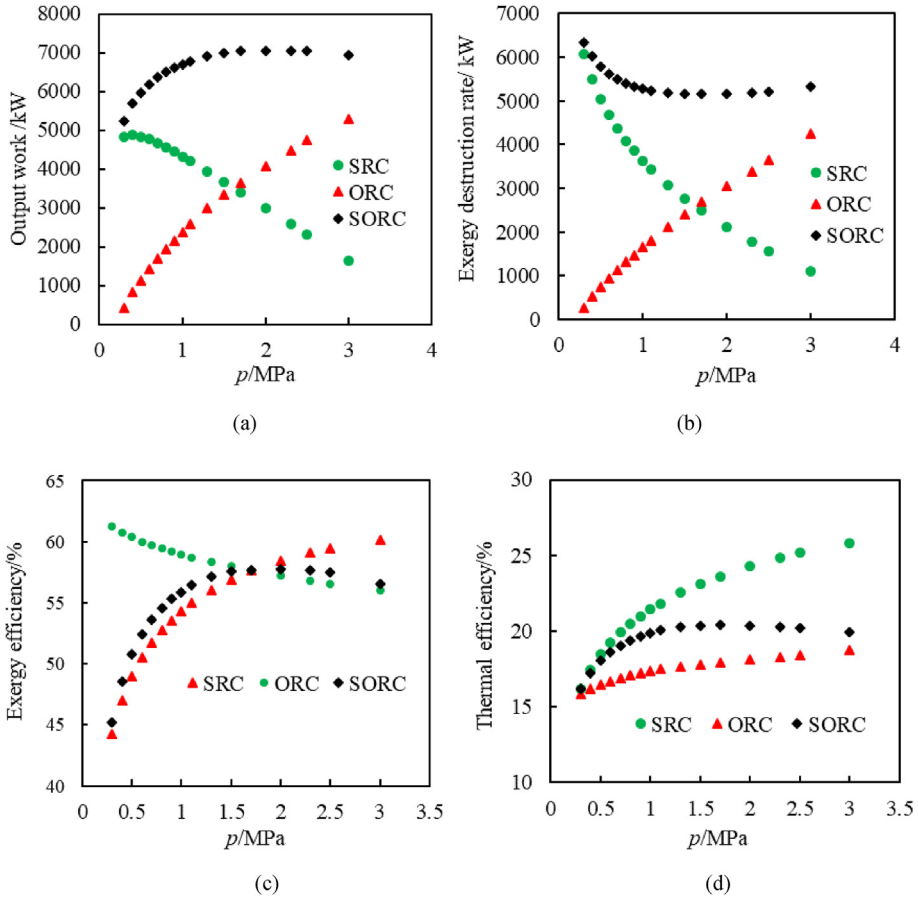

Fig. 3. Variations of thermodynamic performance of SORC at different evaporation pressures of SRC subsystem.

work of the ORC subsystem. The output work of SORC increases first and then decreases slightly with the increase of the evaporation pressure of SRC subsystem. It is caused by that the thermal efficiency of the SORC increases first and then decreases slightly with the increase of the evaporation pressure of the SRC subsystem, as shown in Fig. 3(d), which is determined by that as the evaporation pressure increases, the heat absorbed by the SRC decreases and the output work decreases rapidly, and the heat absorbed by the ORC cycle increases, but the ORC efficiency remains lower than the SRC. Fig. 3(b) shows that the exergy destruction rate of the SRC subsystem decreases when the evaporation pressure increases, while the exergy destruction rate of the ORC subsystem exhibits an opposite trend. This can be explained by the smaller temperature difference in Heat Exchanger 1 and the larger temperature difference in Heat Exchanger 2. The exergy destruction rate of the SORC decreases initially and then slightly rises with the increase of the evaporation pressure of the SRC subsystem. The minimum value occurs when the evaporation pressure of the SRC subsystem is between 1.7 and 2.3 MPa. Fig. 3(c) and (d) show that the thermal and exergy efficiencies of the SORC have similar trends with output work as the variations of evaporation pressure.

Fig. 4 shows the effect of the evaporation pressure of the ORC subsystem on the thermodynamic performance of the SORC with $T_B = 210$ °C and $T_{B'} = 140$ °C. Evaporation pressure and degree of superheat of SRC subsystem are set to 2.1 MPa and 25 °C, respectively. It is evident that the change in the ORC evaporation pressure only affects the performance of the ORC subsystem and the SORC. As shown in Fig. 4(a), when the evaporation pressure of the ORC subsystem increases, the output work of the ORC subsystem and the SORC rises first and then decreases. There are two reasons for this: (1) as the evaporation pressure of the ORC subsystem increases, the temperature of the ORC working fluid from heat exchanger 2 increases, which causes higher thermal efficiency of the ORC subsystem; because the thermal efficiency of the SRC has no change, the higher thermal efficiency of the ORC subsystem results in a higher thermal efficiency of the SORC as shown in Fig. 4(d), therefore the output works of the ORC subsystem and the SORC firstly increase; when the extra output work caused by the increment of thermal efficiency is less than the output work loss caused by the decrement of the heat input into the ORC subsystem as the evaporation pressure of the ORC subsystem increases, the output works of the ORC subsystem and the SORC decrease. The output work of the ORC subsystem and the SORC reaches maximum values at a pressure of approximately 0.75 MPa. In addition, Fig. 4(b) and (c) show that the exergy distribution rates of the ORC subsystem and the SORC decrease as the evaporation pressure of the ORC subsystem rises. This is because as the evaporation pressure of the ORC subsystem increases, the temperature difference in heat exchanger 2 decreases, which means a lower exergy distribution rate of the ORC subsystem. The exergy efficiencies of the ORC subsystem and the SORC show rising trends with the increase of evaporation pressure of the ORC subsystem. This is because the exergy distribution rate of the ORC subsystem falls faster than the output work of the ORC subsystem.

Fig. 5 illustrates the effect of the degree of superheat of the SRC (t_{ds}) on the SORC performance when the evaporation pressure of the SRC is 1.7 MPa, and the pinch point temperature in heat exchanger 2, the EG discharge temperature and the degree of

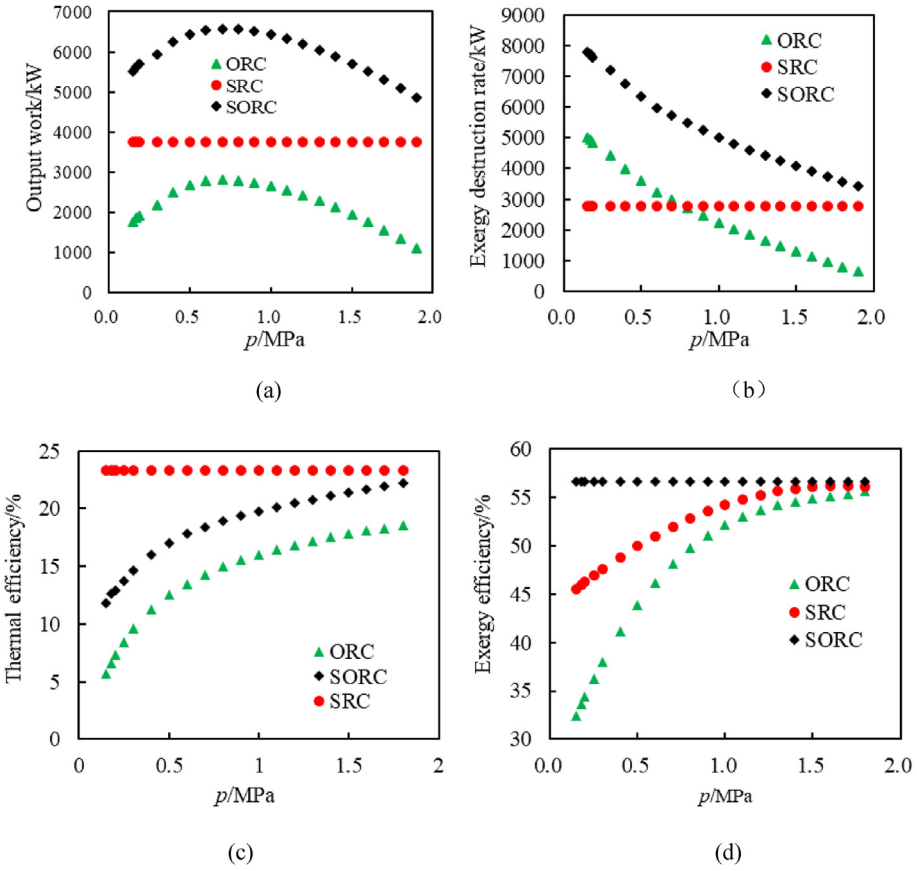

Fig. 4. Variations of thermodynamic performance of SORC at different evaporation pressures of ORC.

superheat are 10 °C, 140 °C, and 25 °C, respectively. As can be observed from Fig. 5 (a), the output work of the SRC tends to decrease when the degree of superheat increases, however it is negligible. Whereas the output works of the ORC and SORC have the opposite tendency. The explanation for this is as the degree of superheat of the SRC increases, there is only a slight increase in the enthalpy of steam at point 3 in the SRC and the combined temperature point (T_B) as shown in Fig. 5 (c). Therefore, the heat input into the SRC has a slight decrease and the heat input into the ORC has a slight increase. The thermal efficiencies of the SRC, ORC and SORC also have minimal increases as shown in Fig. 5(d). As shown in Fig. 5(b), the exergy destruction rates of the SRC and the SORC show a very slight decrease as the degree of superheat of the SRC increases, and the exergy destruction rate of the ORC subsystem shows a very slight increase. It is caused by the higher degree of superheat of the SRC resulting in a smaller temperature difference between the EG and water in heat exchanger 1 while the higher T_B results in a larger temperature difference between the EG and cyclopentane in heat exchanger 2, and the larger temperature difference means a larger exergy destruction rate. Correspondingly, the exergy efficiencies of the SRC and the SORC show very slight increases as the degree of superheat of the SRC increases, while that of the ORC subsystem shows a very slight decrease.

The degree of superheat of the ORC subsystem only affects the performance of the ORC subsystem, so the performance of the ORC subsystem and the SORC has the same trend as the degree of superheat of the ORC changes. Therefore, only the effect of the degree of superheat of the ORC subsystem on the performance of the ORC subsystem was studied. Fig. 6 shows the performance of the ORC subsystem under different degrees of superheat with T_B of 215 °C and evaporation pressure of 1.3 MPa, pinch point temperature in heat exchanger 2 of 10 °C, respectively. As the degree of superheat increases, the output work and the exergy destruction rate of the ORC subsystem has a significant reduction, which is shown in Fig. 6(a) and (b). The reason is that as shown in Fig. 6(c), as the degree of superheat increases, so does the EG discharge temperature, while the temperature difference between the EG and cyclopentane in Heat Exchanger 2 decreases. Therefore, there is less heat input into the ORC subsystem, and a lower exergy destruction rate of Heat Exchanger 2 in the ORC subsystem. As shown in Fig. 6(d), when the degree of superheat of the ORC increases, the thermal efficiency of the ORC subsystem shows a slight increase initially and then a slight decrease. This observation has been noted in other literature (Roy et al., 2011). Because the output work decreases faster than the exergy destruction rate as the degree superheat of the ORC increases, the exergy efficiency of the ORC shows a decreasing tendency, as illustrated in Fig. 6(e).

Using the parameters in Table 2, the maximum output work of the SORC and the contribution of each subsystem under different engine loads with the EG discharge temperature of 140 °C are calculated as shown in Fig. 7. The output work of the ORC subsystem, SRC subsystem and SORC, as well as the contribution of the SRC subsystem to the output work of the SORC are observed to increase as the EG temperature increases which is caused by the increased engine load. As such, it can be deduced that the higher the EG temperature, the more heat input into the SORC, which is mainly input into the SRC subsystem.

Fig. 8 shows the best T_B where the SORC gives the maximum output work as a function of engine EG temperature. The best T_B increases as the temperature of the EG increases, and the increasing

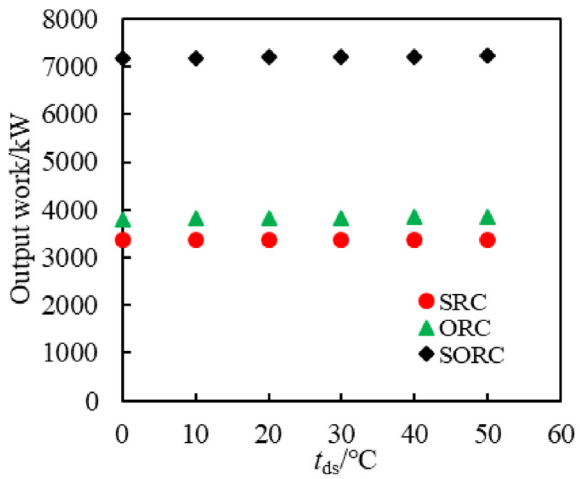

(a)

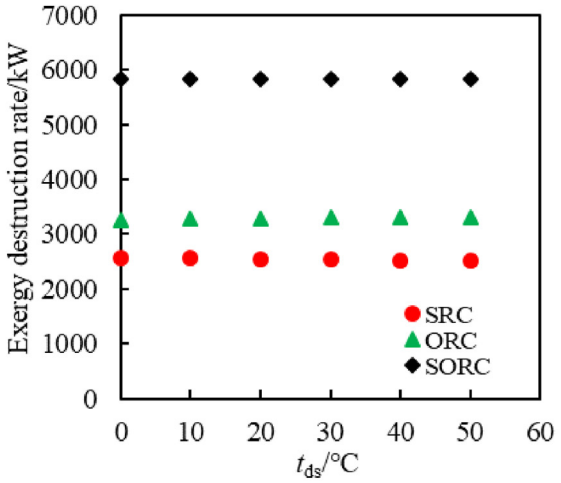

(b)

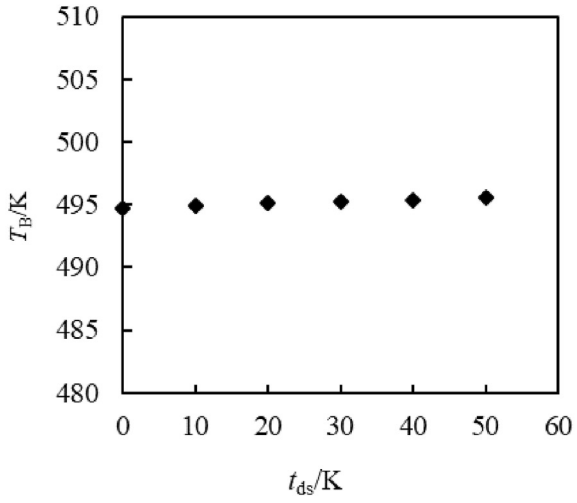

(c)

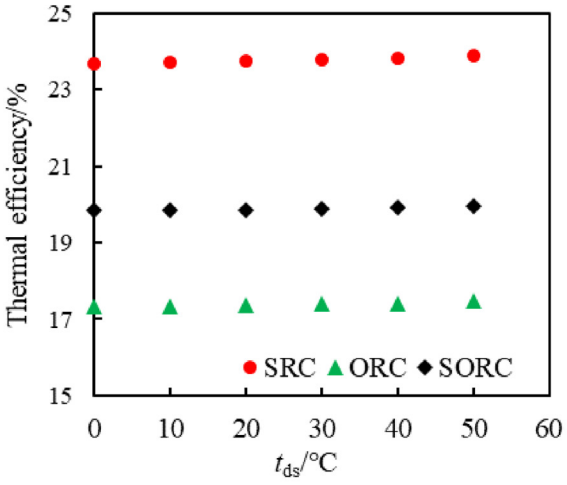

(d)

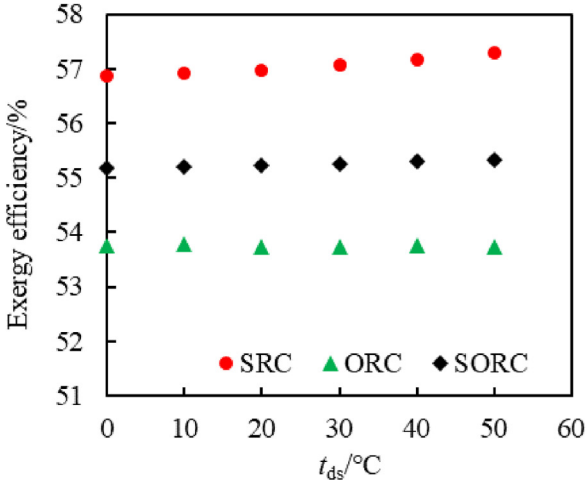

(e)

Fig. 5. Effect of the degree of superheat of SRC on SORC performance.

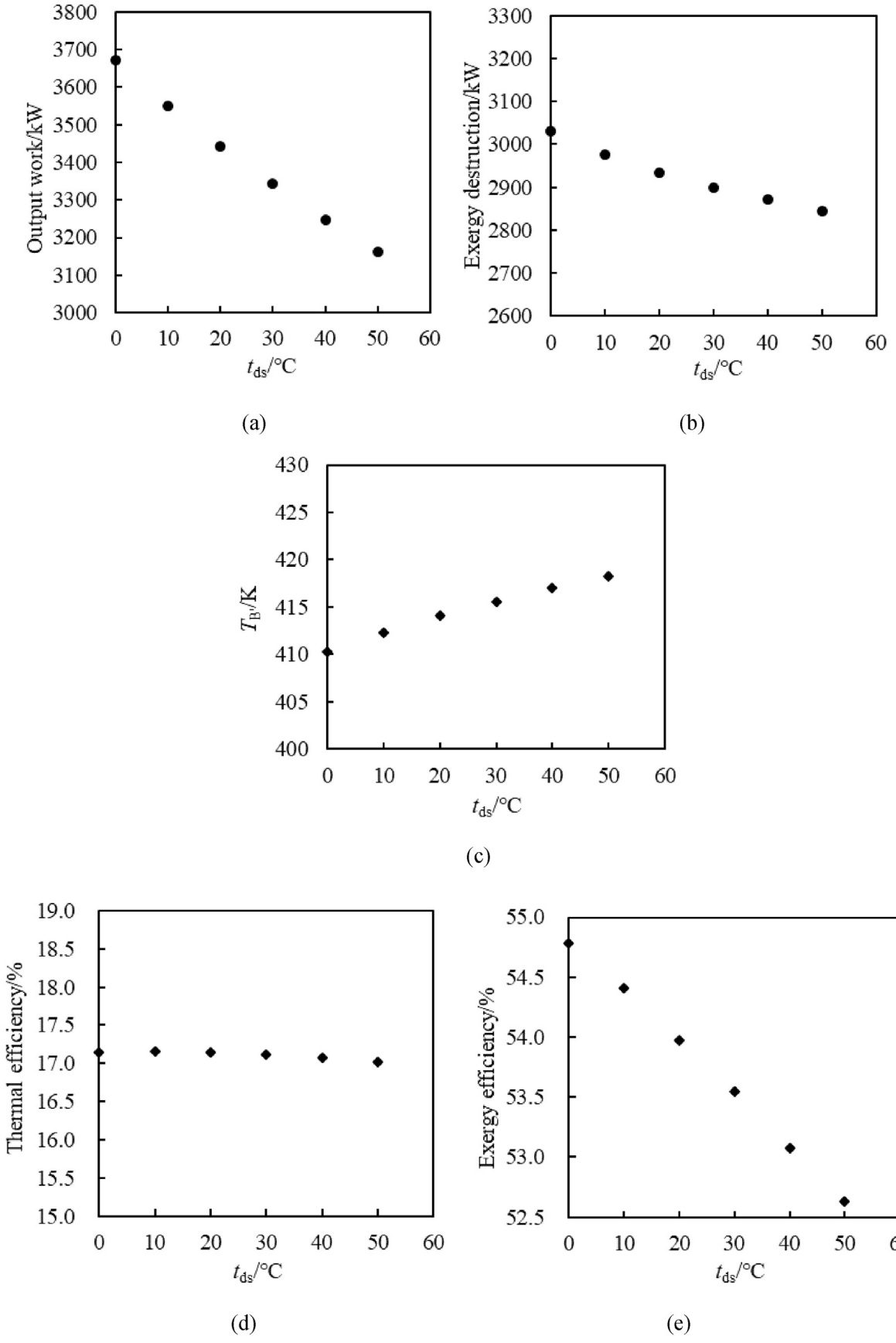

Fig. 6. Effect of degree of superheat of ORC subsystem on the performance of ORC subsystem.

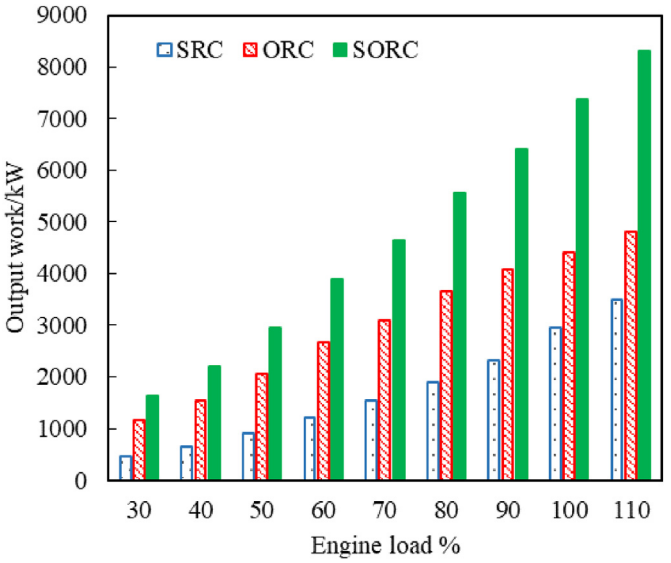

Fig. 7. ORC and SRC contribution ratio in SORC output work.

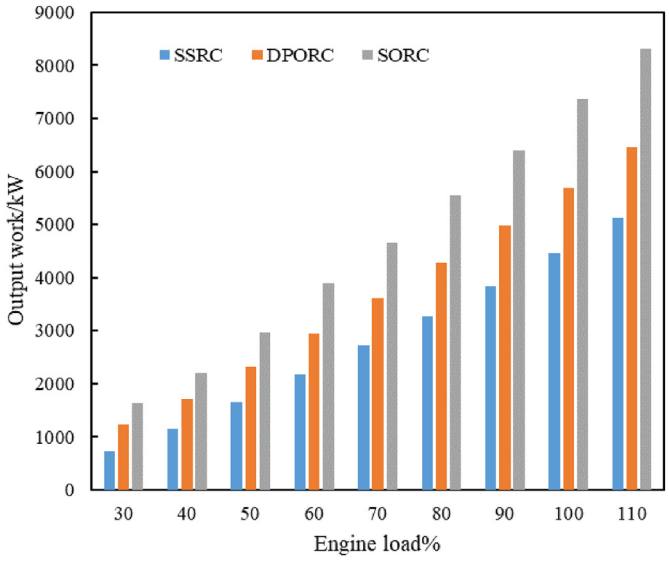

Fig. 10. Comparison of engine waste heat utilization system.

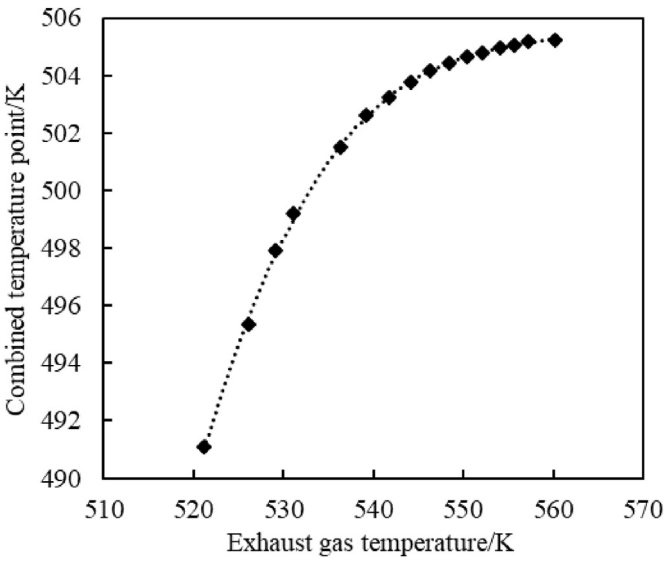

Fig. 8. Effect of EG temperature on the optimal. combined temperature of SRC and ORC.

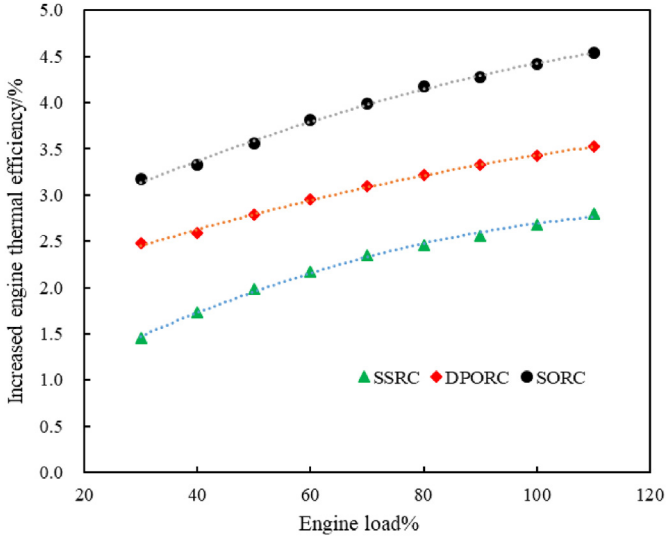

Fig. 11. Comparison of the effects of waste heat utilization systems on the engine thermal efficiency.

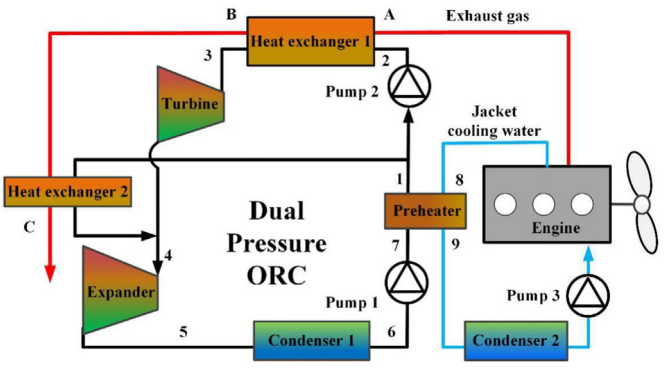

Fig. 9. Schematic diagram of DPORC.

speed becomes significantly slower at approximately 232 °C. This is dependent upon whether the ORC or the SRC subsystem contributes more to the output work.

In order to evaluate the thermodynamic performance of the SORC, the improvements in the output work and the thermal efficiency of the engine from the SORC were compared to those from a single SRC (SSRC) and a dual pressure ORC (DPORC, which is shown in Fig. 9) under different engine loads as shown in Figs. 10 and 11, respectively. The DPORC that was utilized in this comparison is similar to the system designed by Li et al. (2018). In Figs. 10 and 11, the optimized results for SSRC and DPORC are used. It can be determined from Fig. 10 that the output work of the SORC is more than 60% and 27% greater than that of the SSRC and the DPORC, respectively, when the engine load is within the range of 30%–110%. This shows that the SORC recovers more waste heat of the EG

than the SSRC and the DPORC. Additionally, as shown in Fig. 11, the SORC has more than a 60% and 27% in the improvement in thermal efficiency of the engine higher than the SSRC and the DPORC, respectively.

If the ship is in operation 300 days per year under an engine load of 100%, the SORC can generate 52.98 $\times$ 10^6 kWh of electrical power. If the generator efficiency is 176 g·kWh^{-1}, it can save 9322 tons of fuel, which equates to a savings of $10.25 million USD per year based on a fuel price of $1100 USD·ton^{-1}. It should be noted that due to the complexity of the WHRS studied, the findings are more applicable for large ships.

5. Conclusion

This paper proposed a new type of WHRS based on the SRC and ORC to utilize the heat of the EG and the JCW of marine engines. A MAN B&W−14K98 ME/MC marine engine was utilized to evaluate the thermodynamic performance of the WHRS. The main conclusions are as follows:

(1) The output work of the SORC can be improved by decreasing degree of superheat of the ORC subsystem and selecting proper evaporation pressures of ORC subsystem and SRC subsystem. The degree of superheat of the SRC subsystem has no significant effect on the output of work of the SORC.
(2) The output work of SORC increase as engine load increases, which makes the improvement from the SORC on the engine thermal efficiency greater. The best T_B which makes SORC output the maximum work increases as the temperature of EG increases, and the increasing speed becomes significantly slower at approximately 232 °C.
(3) The proposed system can more efficiently utilizing the heat of the EG and JCW of marine engine compared to the existing system. In addition, a portion of the JCW is used as the working fluid of the SRC subsystem, which averts a weight increase of the ship caused by extra water. It is worth mentioning that the proposed system is more applicable for large ships to provide electric power, future work on cogeneration system can be conducted to meet the different remands on ship as well as make better use of waste heat.

Declaration of competing interest

The authors declare that they have no known competing financial interests or personal relationships that could have appeared to influence the work reported in this paper.

CRediT authorship contribution statement

Xiangyang Liu: Conceptualization, Methodology, Writing - review & editing. **Manh Quang Nguyen:** Software, Data curation, Writing - original draft. **Jianchu Chu:** Software, Validation. **Tian Lan:** Investigation, Writing - review & editing. **Maogang He:** Supervision, Writing - review & editing.

Acknowledgments

The supports for the present work provided by the National Natural Science Foundation of China (No. 51525604 and No.51721004), and 111 Project (No. B16038) are gratefully acknowledged.

References

MAN B&W K98ME-C7.1-TII, 2014. Project guide electronically controlled two stroke engines. https://marine.manes.com/applications/projectguides/2stroke/content/printed/K98ME-C7_1.pdf.
Andreasen, J.G., Larsen, U., Haglind, F., 2015. Design of organic Rankine cycles using a non-conventional optimization approach. In: 28th International Conference on Efficiency, Cost, Optimization, Simulation and Environmental Impact of Energy Systems.
Andreasen, J.G., Meroni, A., Haglind, F., 2017. A comparison of organic and steam Rankine cycle power systems for waste heat recovery on large ships. Energies 10 (4), 547.
Baldasso, E., Andreasen, J.G., Mondejar, M.E., et al., 2019. Technical and economic feasibility of organic Rankine cycle-based waste heat recovery systems on feeder ships: impact of nitrogen oxides emission abatement technologies. Energy Convers. Manag. 183, 577−589.
Choi, B.C., Young, M.K., 2013. Thermodynamic analysis of a dual loop heat recovery system with trilateral cycle applied to exhaust gases of internal combustion engine for propulsion of the 6800 TEU container ship. Energy 58, 404−416.
Corbett, J.J., Winebrake, J.J., Green, E.H., et al., 2007. Mortality from ship emissions: a global assessment. Environ. Sci. Technol. 41 (24), 8512−8518.
Ghaebi, H., Namin, A.S., Rostamzadeh, H., 2018. Exergoeconomic optimization of a novel cascade Kalina/Kalina cycle using geothermal heat source and LNG cold energy recovery. J. Clean. Prod. 189, 279−296.
Girgin, I., Ezgi, C., 2017. Design and thermodynamic and thermoeconomic analysis of an organic Rankine cycle for naval surface ship applications. Energy Convers. Manag. 148, 623−634.
He, M., Zhang, X., Zeng, K., et al., 2011. A combined thermodynamic cycle used for waste heat recovery of internal combustion engine. Energy 36, 6821−6829.
Jankowski, M., Borsukiewicz, A., Szopik-Depczyńska, K., et al., 2019. Determination of an optimal pinch point temperature difference interval in ORC power plant using multi-objective approach. J. Clean. Prod. 217, 798−807.
Larsen, U., Nguyen, T.V., Knudsen, T., et al., 2014. System analysis and optimisation of a Kalina split-cycle for waste heat recovery on large marine diesel engines. Energy 64, 484−494.
Li, J., Ge, Z., Duan, Y., Yang, Z., et al., 2018. Parametric optimization and thermodynamic performance comparison of single-pressure and dual-pressure evaporation organic Rankine cycles. Appl. Energy 217, 409−421.
Liu, X., Zhu, C., Yang, F., et al., 2019a. Experimental and correlational study of isobaric molar heat capacities of fatty acid esters: ethyl nonanoate and ethyl dodecanoate. Fluid Phase Equil. 479, 47−51.
Liu, X., Ye, Z., Bai, L., et al., 2019b. Performance comparison of two absorption-compression hybrid refrigeration systems using R1234yf/ionic liquid as working pair. Energy Convers. Manag. 181, 319−330.
Liu, X., Wang, T., He, M., 2019c. Investigation on the condensation process of HFO refrigerants by molecular dynamics simulation. J. Mol. Liq. 111034.
Liu, X., Nguyen, M.Q., Xue, S., et al., 2019d. Vapor−liquid equilibria and interdiffusion coefficients for working pairs for absorption refrigeration systems composed of [HMIM][BF_4] and fluorinated propanes. Int. J. Refrig. 104, 34−41.
Mondejar, M.E., Andreasen, J.G., Pierobon, L., et al., 2018. A review of the use of organic Rankine cycle power systems for maritime applications. Renew. Sustain. Energy Rev. 91, 126−151.
Ng, C.W., Tam, I.C.K., Wu, D., 2019. System modelling of organic rankine cycle for waste energy recovery system in marine applications. Energy Procedia 158, 1955−1961.
Nielsen, R.F., Haglind, F., Larsen, U., 2014. Design and modeling of an advanced marine machinery system including waste heat recovery and removal of sulphur oxides. Energy Convers. Manag. 85, 687−693.
Parikhani, T., Gholizadeh, T., Ghaebi, H., et al., 2019. Exergoeconomic optimization of a novel multigeneration system driven by geothermal heat source and liquefied natural gas cold energy recovery. J. Clean. Prod. 209, 550−571.
Patel, B., Desai, N.B., Kachhwaha, S.S., et al., 2017. Thermo-economic analysis of a novel organic Rankine cycle integrated cascaded vapor compression−absorption system. J. Clean. Prod. 154, 26−40.
Roy, J.P., Mishra, M.K., Misra, A., 2011. Performance analysis of an Organic Rankine Cycle with superheating under different heat source temperature conditions. Appl. Energy 88 (9), 2995−3004.
Salmi, W., Vanttola, J., Elg, M., et al., 2017. Using waste heat of ship as energy source for an absorption refrigeration system. Appl. Therm. Eng. 115, 501−516.
Shu, G., Liang, Y., Wei, H., et al., 2013. A review of waste heat recovery on two-stroke IC engine aboard ships. Renew. Sustain. Energy Rev. 19, 385−401.
Shu, G., Liu, P., Tian, H., et al., 2017. Operational profile based thermal-economic analysis on an Organic Rankine cycle using for harvesting marine engine's exhaust waste heat. Energy Convers. Manag. 146, 107−123.
Singh, D.V., Pedersen, E., 2016. A review of waste heat recovery technologies for maritime applications. Energy Convers. Manag. 111, 315−328.
Soffiato, M., Frangopoulos, C.A., Manente, G., et al., 2015. Design optimization of ORC systems for waste heat recovery on board a LNG carrier. Energy Convers. Manag. 92, 523−534.
Song, J., Song, Y., Gu, C.W., 2015. Thermodynamic analysis and performance optimization of an Organic Rankine Cycle (ORC) waste heat recovery system for marine diesel engines. Energy 82, 976−985.
Theotokatos, G., George, L., 2013. Techno-economical analysis of single pressure exhaust gas waste heat recovery systems in marine propulsion plants. Proc. IME

M J. Eng. Marit. Environ. 227, 83–97.
Uusitalo, A., Honkatukia, J., Turunen-Saaresti, T., et al., 2018. Thermodynamic evaluation on the effect of working fluid type and fluids critical properties on design and performance of Organic Rankine Cycles. J. Clean. Prod. 188, 253–263.
Uusitalo, A., Nerg, J., Grönman, A., et al., 2019. Numerical analysis on utilizing excess steam for electricity production in cruise ships. J. Clean. Prod. 209, 424–438.
Yang, M.H., 2016. Optimizations of the waste heat recovery system for a large marine diesel engine based on transcritical Rankine cycle. Energy 113, 1109–1124.
Yang, M.H., Yeh, R.H., 2015. Thermo-economic optimization of an organic Rankine cycle system for large marine diesel engine waste heat recovery. Energy 82, 256–268.
Zhang, H., Guan, X., Ding, Y., et al., 2018. Emergy analysis of Organic Rankine Cycle (ORC) for waste heat power generation. J. Clean. Prod. 183, 1207–1215.
Zhu, Y., Li, W., Sun, G., et al., 2018. Thermo-economic analysis based on objective functions of an organic Rankine cycle for waste heat recovery from marine diesel engine. Energy 158, 343–356.